The Cryosphere Discuss., 9, 6187–6222, 2015
www.the-cryosphere-discuss.net/9/6187/2015/
doi:10.5194/tcd-9-6187-2015

The Cryosphere Discussions
Open Access
EGU

Antarctic slush-ice algal accumulation not quantified through conventional satellite imagery: Beware the ice of March

J. L. Lieser[1], M. A. J. Curran[1,2], A. R. Bowie[1,3], A. T. Davidson[2], S. J. Doust[2], A. D. Fraser[4,1], B. K. Galton-Fenzi[1,2], R. A. Massom[1,2], K. M. Meiners[1,2], J. Melbourne-Thomas[1,2], P. A. Reid[5], P. G. Strutton[3,6], T. R. Vance[1], M. Vancoppenolle[7], K. J. Westwood[1,2], and S. W. Wright[1,2]

[1]Antarctic Climate & Ecosystems Cooperative Research Centre, University of Tasmania, Private Bag 80, 7001 Hobart, Australia
[2]Australian Antarctic Division, Channel Highway, 7050 Kingston, Tasmania, Australia
[3]Institute for Marine and Antarctic Studies, University of Tasmania, Private Bag 129, 7001 Hobart, Tasmania, Australia
[4]Institute of Low Temperature Science, Hokkaido University, Sapporo, Hokkaido, 060-0819, Japan
[5]Bureau of Meteorology (CAWCR), G.P.O. Box 727, 7001 Hobart, Tasmania, Australia
[6]Australian Research Council Centre of Excellence for Climate System Science, University of Tasmania, 7001 Hobart, Tasmania, Australia

[7]Laboratoire d'Océanographie et du Climat (Expérimentations et Approches Numériques), L'OCÉAN – UMR7159 CNRS/IRD/UPMC/MNHN, IPSL Bote 100, 4 Place Jussieu, 75252 Paris CEDEX 05, France

Received: 17 September 2015 – Accepted: 27 October 2015 – Published: 11 November 2015

Correspondence to: J. L. Lieser (jan.lieser@utas.edu.au)

Published by Copernicus Publications on behalf of the European Geosciences Union.

Abstract

Our current knowledge of broad-scale patterns of primary production in the Southern Ocean is derived from satellite ocean-colour estimates of chlorophyll *a* (Chl *a*) in the open ocean, typically in spring-summer. Here, we provide evidence that large-scale intra-ice phytoplankton surface aggregation occur off the coast of Antarctica during austral autumn, and that these "blooms" are largely undetected in satellite ocean-colour time series (which mask the ice-covered ocean). We present an analysis of (i) true-colour (visible) satellite imagery in combination with (ii) conventional ocean-colour data, and (iii) direct sampling from a research vessel, to identify and characterise a large-scale intra-ice algal occurrence off the coast of East Antarctica in early autumn (March) 2012. We also present evidence of these autumn "blooms" in other regions (for example, Princess Astrid Coast in 2012) and other years (for example, Terra Nova Bay in 2015) implying regular and widespread occurrence of these phenomena. The occurrence of such undetected algal accumulations implies that the magnitude of primary production in the Southern Ocean is currently underestimated.

1 Introduction

In Antarctica, phytoplankton blooms are typically observed during spring and summer in the vicinity of the sea ice edge as it recedes (Arrigo et al., 2008a), and can also occur within the sea ice itself (Massom et al., 2006). Broad-scale assessment of primary production is derived from satellite estimates of Chl *a* based on ocean-colour observations in the open ocean. However, ice-covered regions are masked in the processing (Massom et al., 2006; Bélanger et al., 2007).

In autumn, phytoplankton production declines in the Antarctic sea-ice zone due to limitation of growth by seasonal changes in light and temperature. Declining solar elevations reduce incoming photosynthetically active radiation (PAR); reduced stratification allows deeper mixing of phytoplankton to depths with little light; and declining

TCD
9, 6187–6222, 2015

temperatures allow sea ice to reform, further attenuating light entering the ocean (e.g. Mitchell and Holm-Hansen, 1991; Kang and Fryxell, 1993; Smith Jr. et al., 2000; Arrigo et al., 2008b; Arrigo and Lizotte, 2010).

Using cloud-free data from NASA's TERRA satellite MODIS (MODerate resolution Imaging Spectrometer) true-colour bands 1, 2 and 4 (645, 859 and 555 nm), we detected a large-scale region (~ 30 000 km^2) of ice-associated phytoplankton surface accumulation that developed between 21 February and 19 March 2012 (in the early autumn) off Cape Darnley, East Antarctica, centred on 67.5° S, 70° E (Fig. 1a, a polynya region during winter). The phytoplankton accumulation was not detected in conventional maps of Chl *a* from the MODIS ocean-colour bands (443, 488 and 551 nm). This intense early autumn phytoplankton occurrence, which we suggest was caused by a unique combination of physical and biological processes, challenges the assumption that primary production is negligible in this region during early autumn (Smith Jr. et al., 2000). While we were able to perform some opportunistic sampling, this was insufficient to conclusively establish whether this was a conventional phytoplankton bloom. However, such was the extraordinary concentration of phytoplankton within the sea-ice matrix, as observed from space and on the surface, that we use the term intra-ice "bloom".

Autumn blooms in consolidated sea ice have been observed around Antarctica previously (Fritsen et al., 1994), including in the interior parts of ice floes in the pack ice zone (Meiners et al., 2012). However, these blooms were relatively small in scale and of low intensity. Increased autumn phytoplankton biomass has been observed in association with coastal polynyas around East Antarctica (Arrigo et al., 2015; Arrigo and van Dijken, 2003) and has been inferred from ice core records (Curran et al., 2002) or hypothesised from models of ice-algal production (see for example Appendix A). Late summer blooms have also been reported from Antarctic waters (e.g. Comiso et al., 1990; Smith Jr. and Nelson, 1990), but only where the recent disappearance of sea ice has belatedly exposed coastal waters to high light levels. In this study, we provide first evidence that enhanced concentration of ice-associated phytoplankton occurs in

TCD
9, 6187–6222, 2015

autumn, and that this is not accounted for in current satellite-based Antarctic primary production estimates.

2 Material and methods

2.1 Chronology of 2012 ice-slush phytoplankton event

Daily MODIS true-colour images (pseudo animation in Appendix B) show that initiation of the observed phytoplankton were associated with break-up of landfast sea ice (fast ice) to the east of Cape Darnley between 10 February and 10 March 2012. The initial stages were detected close to this disintegrating fast ice. As the phytoplankton occurrence expanded in scale, it discoloured the sea ice (Fig. 2), which likely consisted of a mixture of pulverised existing ice and newly-formed ice (Massom et al., 2006). This ice was transported by the winds, first to the south (particularly in western Prydz Bay) and then to the north (relevant atmospheric model output can be found in Appendix C) with the change in wind direction occurring around 27 February. We also note evidence of wind-driven strips and patches of sea ice at the southern edge of the "bloom", visible as southeast-northwest aligned streaks west of Cape Darnley around 12 March. This process is presumably driven by katabatic winds.

2.2 Water sampling

On 5 March 2012, seven opportunistic seawater samples were taken in the vicinity of the "bloom" by the research and supply vessel *Aurora Australis* from the uncontaminated seawater line intake system at ~4.8 m depth (see Fig. 1 for the ship track and sampling location). Photos (Fig. 2) suggest a very high biomass of ice-associated algae at the sea surface. Sampling sites were located both within and just outside the bloom region, as identified from MODIS true-colour imagery. Samples were preserved with 1 % vol : vol Lugol's iodine and stored in glass bottles in the dark at 4 °C. Protists were identified using an inverted microscope at 400 and 640 × magnification, and counted

TCD
9, 6187–6222, 2015

in 20 randomly chosen fields of view using a Whipple grid. Cell abundances were converted to biovolumes using the formulae of Hillebrand et al. (1999) and Cornet-Barthaux et al. (2007). Cell carbon values were then calculated from biovolumes using the conversions of Menden-Deuer and Lessard (2000) and Cornet-Barthaux et al. (2007).

2.3 Evidence of ice-associated phytoplankton occurrence in autumn for other years

The early autumn, ice-associated phytoplankton phenomenon documented here is not an isolated event in this region. Using MODIS true-colour data, we identified six other years since February 2000 when ice-associated early autumn blooms occurred in the same region: 2000, 2002, 2005, 2006, 2007, 2008 and 2012 (http://lance-modis.eosdis.nasa.gov/cgi-bin/imagery/realtime.cgi). These blooms are generally most pronounced around 1 March ± 5 days, suggesting a regular mechanism, which we explore below.

3 Results and discussion

3.1 Biological characteristics of the seawater samples

Seawater samples taken on 5 March 2012 indicated differences in the abundance, composition and size of the phytoplankton at sites inside and outside the bloom (Table D1). Concentrations of Chl *a* inside the bloom (2.11 mg m^{-3} average, 3.3 mg m^{-3} maximum) were three to five times higher than those outside the bloom (0.66 mg m^{-3}). Total protist abundance reached 2.6 × 10^{6} cells dm^{-3} in the midst of the bloom compared to 1.2 to 1.7 × 10^{6} cells dm^{-3} outside. Ice-associated phytoplankton abundance at the surface could have been larger than at 4.8 m depth, but unfortunately could not be measured at the time.

TCD
9, 6187–6222, 2015

Overall, our results show that the phytoplankton biomass was higher in the bloom due to higher densities and the large cell size of the dominant taxa. The phytoplankton community was dominated by members of the diatom genus *Fragilariopsis*, which comprised 56 to 75 % of all autotrophs sampled. The absolute abundance of *Fragilariopsis* spp. differed little between sampling sites, but cells sampled within the bloom were larger (most 20 to 50 µm long, with some up to 80 µm long) compared to cells outside (commonly < 10 µm long). The haptophyte *Phaeocystis antarctica* was the second most abundant taxon, averaging 18 % of all autotrophs by number and reaching 3.1×10^5 cells dm^{-3} at both ice-covered and ice-free locations. Cell concentrations did not vary systematically with ice cover but their small size (~ 2 to 5 µm in diameter) meant they contributed little to overall protistan biomass. Phytoplankton taxa that inhabit sea ice, namely *Entomoneis* sp. and *Polarella glacialis*, were also present at low abundances within the bloom but were absent outside (Table D1).

3.2 Underestimated importance of ice-associated phytoplankton in autumn

The ice-associated phytoplankton in the region off Cape Darnley was not detected in conventional satellite ocean-colour images. Figure 1a shows MODIS level 2 Chl *a* data in the Cape Darnley region, East Antarctica, acquired on 2 March 2012 10:30 UTC. The highest values are at the fringe of the area that was masked by sea ice and/or cloud cover, and scattered within that region. The MODIS true-colour composite has been overlaid in regions where sea ice and/or cloud cover prohibited Chl *a* retrievals, and the discoloured sea ice and ice slush is obvious in Fig. 1a. A ship-borne image (taken 5 March 2012) of the sea ice/slush matrix is given in Fig. 2. In this region, the combination of different products from the same MODIS instrument (Fig. 1a) demonstrates that satellite-derived estimates of Chl *a* are lower than actual values. Also included in Fig. 1a is the ship's track while sampling the bloom three days later. This track shows Chl *a* calculated from underway fluorometry samples with the highest values of up to 3 mg m^{-3} inside the bloom area, matching the highest values of the remote sensing Chl *a* estimates along the edges of the detection. Figure 1b demonstrates the close

TCD
9, 6187–6222, 2015

agreement between remote sensing data and samples in an along-track view where the satellite data are not masked by sea ice and/or clouds, and the high values of Chl *a* of up to 6 mg m^{-3} inside the masked area of the bloom patch. Because they have not been detected in the past, large-scale autumn blooms within the sea ice zone have not been factored into calculations of regional-scale primary production for the Southern Ocean (e.g. Arrigo et al., 2008b). These results are evidence that ice-associated phytoplankton production is underestimated in other seasons too (e.g. Massom et al., 2006; Massom and Stammerjohn, 2010).

3.3 Proximal drivers of bloom formation in autumn

We hypothesise that the combination of five environmental variables create the conditions that lead to this early autumn bloom formation; sea ice, winds, light, nutrient availability and lack of grazing pressure (see conceptual representation shown in Fig. 3a). In early March, the interaction of these variables allows for an environmental window in which these ice-associated blooms can form (Fig. 3b), as follows.

3.3.1 Sea ice conditions

Based on the MODIS time series and information in Fig. 2, this early-autumn "bloom" appears to be associated with the decay of fast ice and new sea-ice formation. Sea-ice growth in the Cape Darnley region typically begins in late February to early March (Massom et al. (2013) and Fig. 3b), driven by the air-sea temperature gradient and winds. Frazil ice formation can act to concentrate phytoplankton in the newly-forming sea ice matrix, with frazil crystals "scavenging" algal cells from the water column as they rise (Garrison et al., 1983). One-dimensional biophysical model simulations (detailed in Appendix A) suggest that frazil scavenging (Garrison et al., 1989) is not essential to Chl *a* accumulation in the ice, but would accelerate it. MODIS ocean-colour imagery indicates that there was chlorophyl in the same region prior to initiation of the ice-associated bloom (see Fig. E1), possibly as a result of decay of fast ice. Fast ice

TCD
9, 6187–6222, 2015

decay occurs through break-up and pulverisation by wind and wave activity. That decay releases both concentrated algal cells and nutrients to the surrounding ice slush (Massom et al., 2006). We suggest that concentrated phytoplankton cells, within this interstitial sea ice matrix between brash ice and floes, comprise the discolouration of sea ice observed in MODIS true-colour imagery (Fig. 1a) and from the ship (Fig. 2).

3.3.2 Wind conditions

Strong winds in the Cape Darnley region in March 2012 are indicated in the high-resolution polar realisation ACCESS-P model output (Appendix C). Such conditions (Fig. 3b) favour both the break-up and pulverisation of fast ice, and the formation of new and frazil ice. Wind action may also play a key role delivering nutrients by aeolian transport (Winton et al., 2014) from the continent, as well as increasing the spatial extent by dispersion of the bloom throughout its lifetime.

3.3.3 Light

At the high latitude at which the bloom was observed in March, the availability of incoming PAR is sufficient to initiate bloom conditions if phytoplankton are confined to a shallow ice-slush matrix on the surface. In this way, they are exposed to higher light levels than is the case in ice-free areas where deeper mixing can result in light limitation, or within consolidated sea ice with a snow cover where snow significantly attenuates PAR (Massom et al., 2006). At such a low light angle, sea ice also acts to trap and scatter the light which the phytoplankton can use (Buckley and Trodahl, 1987).

3.3.4 Nutrient availability

Primary production in the Southern Ocean is strongly limited by the availability of nutrients (Blain et al., 2007). Following spring blooms, the exhaustion of nutrients, particularly iron, together with increased grazing pressure and decreased stratification leads to a decline in production in the open ocean (de Baar et al., 1995).

TCD
9, 6187–6222, 2015

In the region of the Cape Darnley bloom, the presence of large diatoms is consistent with iron enrichment (Coale et al., 2004). Sea ice and fast ice has been shown to contain high concentrations of iron relative to adjacent areas of open water (van der Merwe et al., 2011), so its subsequent pulverisation by waves likely released iron in the bloom region, to initiate or maintain algal growth.

Other potential sources of iron to support this early autumn bloom include: iceberg melt, wind-driven snow deposition, perhaps containing iron-rich dust, from the continent and wind-driven upwelling (see Fig. F1). Of these, iceberg sources of nutrients are difficult to quantify for the Cape Darnley bloom, but fast ice break-up was observed and upwelling can be inferred from wind strength and direction. Fast ice break-up in western Prydz Bay was observed in MODIS true-colour imagery ten days before the detection of the ice-associated bloom (Appendix B).

3.3.5 Grazing

Within the bloom region, the habitat provided by sea ice provides a protective matrix against zooplankton grazing (Krembs et al., 2000). Microbial grazers, such as heterotrophic flagellates, dinoflagellates and ciliates, were more abundant in the bloom, but their grazing was insufficient to limit phytoplankton growth. In the absence of samples to indicate metazoan grazer densities, it is not possible to quantify total grazing pressure for the ice-associated bloom.

3.4 Climate indices

The discovery of this bloom and the satellite-based evidence of other such blooms in different years and regions, and implications for primary production estimates, raises the question of inter-annual variability. Our initial investigation suggests that the positive phase of El Niño-Southern Oscillation (ENSO) and the Southern Annular Mode (SAM) may play a role (see discussion in Appendix G). Understanding these drivers of

TCD
9, 6187–6222, 2015

inter-annual variability, and their association with blooms of this type, is important for estimating the scale of this additional source of primary production.

4 Conclusions

This intra-ice phytoplankton "bloom" appears to be the consequence of a combination of sea ice conditions resulting from breakup of fast ice and initial growth stages of new sea ice. We suggest that the combination of sufficient light, nutrients released from disintegrating ice, subsequent wind redistribution and a reduction in grazing pressure allows for this phytoplankton bloom. Blooms of this type are a potentially important source of primary production in the Southern Ocean, which is not currently quantified with ocean-colour remote sensing, and therefore have implications for Southern Ocean food webs and biogeochemical cycling (Murphy et al., 2012).

Appendix A: One-dimensional bio-physical model results

The model couples a simple N-P module with the halo-thermodynamic model (Vancoppenolle et al., 2010). This model captures ice thermodynamics, halo-dynamics, a radiation scheme, and a simple nutrient-phytoplankton ice algae model, characterised by one species of ice algae (diatoms) and two limiting nutrients (nitrates and silicates). Provided that iron is plentiful, the algal biomass observed in MODIS true-colour imagery and in-situ (from the research vessel *Aurora Australis*) originates either from (i) in-ice growth of algae, or (ii) scavenging of algal cells from the water column by rising frazil ice crystals. These alternative hypotheses were tested using simple calculations and model simulations.

TCD
9, 6187–6222, 2015

A1 Simple calculations

A1.1 In-ice growth of ice algae

We first compute the amount of Chl *a* that is achievable from the in-situ growth of ice algae by consumption of the the locally available nutrients. Assuming that 30 % of the oceanic concentration of silicates of $C_i^{Si} = 40\,\mathrm{mmol\,m^{-3}}$ is stored in the sea ice during formation (the rest being rejected by brine gravity drainage) and fully exhausted by ice algae, then we get that chlorophyll *a* concentration in sea ice is:

$$C_i^{\mathrm{Chl}\,a} = r_{\mathrm{C}}^{\mathrm{Chl}\,a}\, r_{\mathrm{Si}}^{\mathrm{C}}\, C_i^{\mathrm{Si}} \times 30\,\% \approx 17\,\mathrm{mg\ Chl}\,a\,\mathrm{m^{-3}} \tag{A1}$$

where $r_{\mathrm{C}}^{\mathrm{Chl}\,a} = 0.15\,\mathrm{mg\,mmol^{-1}}$ is a standard chlorophyll : carbon ratio in sea ice diatoms and $r_{\mathrm{Si}}^{\mathrm{C}} = 9.09$ is the C : Si molar ratio (Sarthou et al., 2005).

A1.2 Scavenging of frazil crystals

The Cape Darnley post-polynya is highly productive in late summer (see Arrigo and van Dijken, 2003), with surface Chl *a* concentrations reaching up to 5 mg Chl *a* $\mathrm{m^{-3}}$. Assuming that a fraction $\alpha = 10\,\%$ of seawater Chl *a* with a concentration $C_o^{\mathrm{Chl}\,a} = 1\,\mathrm{mg\,m^{-3}}$ is scavenged by raising frazil crystals over an oceanic depth of $h_o = 50\,\mathrm{m}$, the resulting average Chl *a* concentration in 30 cm thick sea ice should be:

$$C_i^{\mathrm{Chl}\,a} = \frac{\alpha C_o^{\mathrm{Chl}\,a} h_o}{h_i} \approx 17\,\mathrm{mg\ Chl}\,a\,\mathrm{m^{-3}}. \tag{A2}$$

These two scenarios give equivalent (high) Chl *a* concentrations and do not distinguish between our two hypotheses for the bloom source.

TCD
9, 6187–6222, 2015

A2 Model simulations

The model is designed to represent un-deformed level (columnar) ice, we apply it here to the sea ice mixture that characterised the Cape Darnley early autumn bloom. This is based on the assumption that nutrient pathways in level ice (e.g. brine channels) that are captured in the one-dimensional model, behave similarly to the frazil mixture found between pancakes (although this mixture likely occupies more volume than brine channels, because of the constant swell forcing that tends to prevent full ice consolidation). As Chl *a* is a particulate tracer, we assume 100 % of incorporation ($C_i^{\mathrm{Chl}\,a} = C_o^{\mathrm{Chl}\,a}$). The model therefore arguably provides a rough, minimal, representation of the Cape Darnley bloom conditions.

Forcing and initial conditions

The sea ice model is forced at boundaries with the following numbers:

- sea surface salinity = 34 g kg^{-1};
- nitrate concentration in seawater = 30 mmol m^{-3} (typical value from that region, see Sarmiento and Gruber, 2006);
- silicate concentration in seawater = 40 mmol m^{-3} (typical value from that region, see Sarmiento and Gruber, 2006);
- atmospheric heat fluxes from empirical formula for sensible, latent, shortwave and long wave fluxes, fed by daily NCEP temperatures, winds and specific humidity (multiplied by 0.83 to correct a known systematic bias), together with a climatology of cloud fraction;
- a prescribed very small snowfall rate.

Model runs start at day-of-year 50 (19 February) when the surface energy budget becomes negatives, which (approximately) corresponds with the onset of ice formation.

TCD
9, 6187–6222, 2015

Runs last 30 days, until day-of-year 80 (20 March), and are initialised with standard thin ice characteristics:

- ice thickness = 5 cm;
- snow depth = 2 cm;
- ice salinity = 22.93 g kg^{-1} (from the formula of Kovacs (1996) giving bulk ice salinity for young ice as a function of its thickness);
- nitrate concentration = 20.23 mmol N m^{-3} (same ice-ocean ratio as for salt);
- silicate concentration = 26.97 mmol Si m^{-3} (same ice-ocean ratio as for salt).

The concentration of carbon stored in ice algae C_i^{DA} is also prescribed at the oceanic boundary (C_o^{DA}). As this concentration in the ocean is used as an initial concentration in forming new ice, accreted at the ice base, we made several sensitivity experiments.

- Exp. 1: $C_o^{DA} = 0.5$ mmol C m^{-3}; $\mu = 1.3 \times 10^{-5}$ s^{-1};
- Exp. 2: $C_o^{DA} = 0.5$ mmol C m^{-3}; $\mu = 1.95 \times 10^{-5}$ s^{-1};
- Exp. 3: $C_o^{DA} = 5$ mmol C m^{-3}; $\mu = 1.3 \times 10^{-5}$ s^{-1};
- Exp. 4: $C_o^{DA} = 50$ mmol C m^{-3}; $\mu = 1.3 \times 10^{-5}$ s^{-1},

where μ is the maximum specific photosynthesis rate.

Experiment 1 corresponds to < 0.1 mg Chl *a* m^{-3} (no biological activity in the ocean). In experiment 2, we tested the role of the maximum specific growth rate μ, which is rather uncertain. It would be bigger if the diatoms are adapted to high-light levels (ocean diatoms) and lower if they are adapted to low-light levels (ice diatoms). In experiment 3, the seawater that sea ice is forming from is typical of bloom conditions (≈ 1 mg Chl *a* m^{-3}), but there is no harvesting of organic matter by frazil crystals. In experiment 4, the seawater is typical of bloom conditions, and we assume that initial

TCD
9, 6187–6222, 2015

concentration in forming ice is enhanced by frazil scavenging (initial concentration of Chl *a* in sea ice ≈ 10 mg Chl *a* m^{-3}).

A3 Results

The model grows 50 cm of ice thermodynamically within the 30 day simulation period (Fig. A1). The cold air temperatures imply low temperatures and high brine salinities in the upper ice, which is improper to ice algae growth, as can be seen from the limitation factors in the lower panels of the Fig. A1 (0 = improper to ice algal growth, 1 = ice algal growth is possible). The four sensitivity experiments give quite different blooms, particularly in terms of Chl *a* concentration and timing of maximum Chl *a* values (Fig. A2). Integrating Chl *a* vertically (Fig. A3a) and dividing by ice thickness to get mean concentrations in sea ice (Fig. A3b) indicates the following differences between experiments:

- Experiment 1 gives low concentrations that are probably unrealistic;
- Experiment 4 (frazil scavenging experiment) gives the fastest ice algal growth rate and the most abundant ice algae;
- Experiments 2 and 3 are in between these extremes. Experiment 2 indicates that light-acclimated diatoms with higher μ might outcompete ice algae in the bloom. The concentrations in sea ice are high and the timing of maximum concentrations (around day-of-year 60) is consistent with observations. Experiment 3 indicates that even without frazil scavenging, accumulation of organic matter from the upper ocean creates a sufficient basis for ice algal growth.

A4 Conclusion

Model simulations suggest that frazil scavenging would lead to rapid and intense ice algal development (Experiment 4). Sensitivity experiments also suggest that substantial activity is possible in the ice (i) with no frazil scavenging but accumulation of surface

TCD
9, 6187–6222, 2015

material in forming ice (Experiment 3); (ii) with no activity in the water, but with light-acclimated diatoms outcompeting ice diatoms in the slush (Experiment 2). On the basis of these results, it is not possible to distinguish between alternative hypotheses for the origin of algal cells in the ice-associated bloom.

Appendix B: Animation of MODIS true-colour imagery

A series of daily MODIS true-colour images is shown in this animation, available from ftp://ftp.acecrc.org.au/pub/jllieser/MODIS_Animation.pps (9.3 MB). The sequence starts with the initiation of the observed occurance on 10 February 2012 und finishes on 10 March 2012.

Appendix C: Link to ACCESS-P winds

Atmospheric model output from ACCESS-P model (Shrestha et al., 2013), with relation to the observed bloom phenomenon can be found at: ftp://ftp.bom.gov.au/anon/home/cawcr/perm/preid/research/algal_bloom/access_p_algal_bloom.html.

Appendix D: Water sample biological characteristics

Sampling sites were located within and outside the region identified from MODIS true-colour imagery as experiencing a bloom. Samples of 1 L were preserved with 1 % vol : vol Lugol iodine and stored in glass bottles in the dark at 4 °C. Protists were identified and counted using phase and Nomarski interference optics using an Olympus IX71 and IX81 inverted microscope at 400 to 640× magnification. Bright field optics was also used to discriminate taxa that contained chloroplasts. Protistan taxa were counted in 20 randomly chosen fields of view, except for highly abundant taxa that were counted in a subset of the field of view defined by an ocular quadrant (Whipple grid).

TCD
9, 6187–6222, 2015

Cell biovolumes and carbon conversion statistics were used to calculate the cell biomass of protistan taxa/groups. The average cell volume of each protistan taxon was calculated using formulae presented by Hillebrand et al. (1999) and Cornet-Barthaux et al. (2007). Cell carbon was then calculated using the volume-specific carbon conversions of Menden-Deuer and Lessard (2000) and Cornet-Barthaux et al. (2007).

Species composition and biomass differed significantly between sampling sites inside and outside the bloom area (PERMANOVA, $P = 0.028$ and $P = 0.026$, respectively) (Anderson et al., 2008). Based on SIMPER analysis (Primer-E Ltd) large diatoms (predominantly *Fragilariopsis*) explained ~ 40 % of the difference based on abundance and > 50 % based on biomass (Clarke and Gorley, 2006). Thus, the observed protistan community within the bloom area differed markedly from the communities in surrounding ice-free areas in terms of composition, abundance and cell size distribution.

Appendix E: Ocean colour image of Cape Darnley region for 11 February 2012

With Fig. E1 we provide a MODIS ocean-colour scene before the ice associated bloom (11 February 2012) to show the existing primary production.

Appendix F: True colour image of Cape Darnley region for 23 February 2012

Figure F1 shows a MODIS true-colour image, illustrating potential ice seeding mechanisms, including (1) wind-driven formation of strips and patches, (2) disintegrating fast ice, and (3) wind-blown snow off the face of the Amery Ice Shelf.

Appendix G: Interactions between ENSO and SAM in the Southern Hemisphere

We identified an association between the years in which ice-associated early autumn blooms were detected in MODIS true-colour imagery for Cape Darnley, and modes of

TCD
9, 6187–6222, 2015

climate variability that influence the Southern Ocean, specifically the El Niño-Southern Oscillation (ENSO) and the Southern Annular Mode (SAM). The Southern Oscillation Index (SOI) is an index describing the atmospheric oscillation between El Niño (warm) and La Niña (cool) temperature states in the tropical eastern Pacific Ocean. Vance et al. (2013) showed that there is a circumpolar ENSO signal in the westerly winds around Antarctica. This strengthening was further enhanced by interaction of ENSO with the SAM. By austral summer in El Niño (La Niña) years, tropospheric anomalies develop into a circumpolar ridge-like (trough-like) anomaly across Antarctica that weakens (strengthens) circumpolar westerlies (Fig. G1) and interacts with the SAM (L'Heureux and Thompson, 2006).

In the Cape Darnley region, these ice-associated early autumn blooms occurred in years when La Niña and positive SAM conditions generated high winds (Fig. G1), which is one of the important drivers identified for this bloom (see Fig. 3b of the original paper). The short satellite dataset (2000–2012) limits our ability to confirm this ENSO-SAM-bloom relationship in a statistically significant way, but it occurs more often than by chance (Fogt et al., 2011) and is likely linked to greenhouse gas forcing (IPCC, 2007). Therefore, these previously unquantified blooms may increase in frequency, further contributing to primary production in the Southern Ocean.

A circumpolar pressure signal of ENSO

The interaction between ENSO and SAM during DJF is primarily the result of coincident La Niña-SAM positive, El Niño-SAM negative or ENSO-weak SAM events occurring more often than by chance (Fogt et al., 2011). Other iterations (i.e. La Niña-SAM negative) resulted in anomalous transient eddies in the mid-latitudes that opposed rather than reinforced the SAM-ENSO interaction. During La Niña-SAM positive events (Fig. G1, upper panel), an anomalous circumpolar trough over the Antarctic continent and coastal regions is paired with a decidedly un-SAM-like zonal wavenumber 3 (ZW3) pattern at mid-latitudes. ZW3 is associated with transitions from strongly meridional to strongly zonal flow (Raphael, 2007). ZW3 is thought to be associated with ENSO, and

TCD
9, 6187–6222, 2015

an Australian sector wave 3 index (AZ3 – van Ommen and Morgan, 2010) is strongly correlated with SOI during summer (Table G1).

The NCEP/NCAR reanalysis (Kistler et al., 2001) was used to investigate GPH anomalies. All reanalysis datasets have high latitude data problems related to data scarcity and trend effects in the Southern Hemisphere, particularly prior to 1979 (Hines et al., 2000; Kistler et al., 2001). Data coverage improves greatly after 1979, thus we used composites from 1979–2009.

The Supplement related to this article is available online at doi:10.5194/tcd-9-6187-2015-supplement.

Acknowledgements. We acknowledge the use of MODIS data products or imagery from the Land, Atmosphere Near real-time Capability for EOS (LANCE) system operated by the NASA/GSFC/Earth Science Data and Information System (ESDIS) with funding provided by NASA/HQ (https://earthdata.nasa.gov). Model data can be obtained on request from M. Vancoppenolle (martin.vancoppenolle@locean-ipsl.upmc.fr). Underway and sample data are available from K. Westwood (Karen.Westwood@aad.gov.au).

We thank Barbara Frankel, Julie McInnes, Fanny Chever, Maurice Levasseur and Martine Lizotte for their work on sample processing and analysis, Nobuo Kokubun (NIPR) for in-situ photography, and So Kawaguchi, Rob King and Tom Trull for their helpful contributions to initial discussions regarding the autumn "bloom". We are grateful to science support staff and crew aboard RSV *Aurora Australis* for making it possible for sampling to occur. Finally we thank Steve Nicol, Ian Allison, Tom Trull, Ian Murray and Rowan Trebilco for constructive comments that greatly improved an early version of the manuscript. This work was supported by the Australian Government's Cooperative Research Centre program through the Antarctic Climate & Ecosystem CRC (ACE CRC). JLL was supported under Australian Research Council's Special Research Initiative for Antarctic Gateway Partnership (Project ID SR140300001).

TCD
9, 6187–6222, 2015

References

Anderson, M. J., Gorley, R. N., and Clarke, K. R.: PERMANOVA+ for PRIMER: guide to software and statistical methods, Tech. rep., Primer-E Ltd., Plymouth, 2008. 6203

Arrigo, K. R. and Lizotte, M. P.: Primary producers in sea ice, in: Sea Ice, 2nd Edn., edited by: Thomas, D. N. and Dieckmann, G. S., Wiley, New York, USA, 283–325, 2010. 6190

Arrigo, K. R. and van Dijken, G. L.: Phytoplankton dynamics within 37 Antarctic coastal polynya systems, J. Geophys. Res., 108, 3271, doi:10.1029/2002JC001739, 2003. 6190, 6198

Arrigo, K. R., van Dijken, G., and Long, M.: Coastal Southern Ocean: A strong anthropogenic CO_2 sink, Geophys. Res. Lett., 35, L21602, doi:10.1029/2008GL035624, 2008a. 6189

Arrigo, K. R., van Dijken, G. L., and Bushinsky, S.: Primary production in the Southern Ocean, 1997–2006, J. Geophys. Res., 113, C08004, doi:10.1029/2007JC004551, 2008b. 6190, 6194

Arrigo, K. R., van Dijken, G. L., and Strong, A. L.: Environmental controls of marine productivity hot spots around Antarctica, J. Geophys. Res.-Oceans, 120, 5545–5565, doi:10.1002/2015JC010888, 2015. 6190

Bélanger, S., Ehn, J. K., and Babin, M.: Impact of sea ice on the retrieval of water-leaving reflectance, chlorophyll a concentration and inherent optical properties from satellite ocean color data, Remote Sens. Environ., 111, 51–68, doi:10.1016/j.rse.2007.03.013, 2007. 6189

Blain, S., Quéguiner, B., Armand, L., Belviso, S., Bombled, B., Bopp, L., Bowie, A., Brunet, C., Brussaard, C., Carlotti, F., Christaki, U., Corbière, A., Durand, I., Ebersbach, F., Fuda, J.-L., Garcia, N., Gerringa, L., Griffiths, B., Guigue, C., Guillerm, C., Jacquet, S., Jeandel, C., Laan, P., Lefèvre, D., Lo Monaco, C., Malits, A., Mosseri, J., Obernosterer, I., Park, Y.-H., Picheral, M., Pondaven, P., Remenyi, T., Sandroni, V., Sarthou, G., Savoye, N., Scouarnec, L., Souhaut, M., Thuiller, D., Timmermans, K., Trull, T., Uitz, J., van Beek, P., Veldhuis, M., Vincent, D., Viollier, E., Vong, L., and Wagener, T.: Effect of natural iron fertilization on carbon sequestration in the Southern Ocean, Nature, 446, 1070–1074, doi:10.1038/nature05700, 2007. 6195

Buckley, R. G. and Trodahl, H. J.: Scattering and absorption of visible light by sea ice, Nature, 326, 867–869, 1987. 6195

Clarke, K. R. and Gorley, R. N.: PRIMER V6: User Manual/Tutorial, Primer-E Ltd., Plymouth, UK, 2006. 6203

TCD
9, 6187–6222, 2015

Coale, K. H., Johnson, K. S., Chavez, F. P., Buesseler, K. O., Barber, R. T., Brzezinski, M. A., Cochlan, W. P., Millero, F. J., Falkowski, P. G., Bauer, J. E., Wanninkhof, R. H., Kudela, R. M., Altabet, M. A., Hales, B. E., Takahashi, T., Landry, M. R., Bidigare, R. R., Wang, X., Chase, Z., Strutton, P. G., Friederich, G. E., Gorbunov, M. Y., Lance, V. P., Hilting, A. K., Hiscock, M. R., Demarest, M., Hiscock, W. T., Sullivan, K. F., Tanner, S. J., Gordon, R. M., Hunter, C. N., Elrod, V. A., Fitzwater, S. E., Jones, J. L., Tozzi, S., Koblizek, M., Roberts, A. E., Herndon, J., Brewster, J., Ladizinsky, N., Smith, G., Cooper, D., Timothy, D., Brown, S. L., Selph, K. E., Sheridan, C. C., Twining, B. S., and Johnson, Z. I.: Southern Ocean iron enrichment experiment: carbon cycling in high- and low-Si waters, Science, 304, 408–411, doi:10.1126/science.1089778, 2004. 6196

Comiso, J. C., Maynard, N. G., Smith, W. O., and Sullivan, C. W.: Satellite Ocean Color Studies of Antarctic Ice Edges, J. Geophys. Res., 95, 9481–9496, 1990. 6190

Cornet-Barthaux, V., Armand, L., and Quéguiner, B.: Biovolume and biomass estimates of key diatoms in the Southern Ocean, Aquat. Microb. Ecol., 48, 295–308, doi:10.3354/ame048295, 2007. 6192, 6203

Curran, M. A., Palmer, A. S., Van Ommen, T. D., Morgan, V. I., Phillips, K. L., McMorrow, A. J., and Mayewski, P. A.: Post-depositional movement of methanesulphonic acid at Law Dome, Antarctica, and the influence of accumulation rate, Ann. Glaciol., 35, 333–339, doi:10.3189/172756402781816528, 2002. 6190

de Baar, H. J. W., de Jong, J. T. M., Bakker, D. C. E., Löscher, B. M., Veth, C., Bathmann, U., and Smetacek, V.: Importance of iron for plankton blooms and carbon dioxide drawdown in the Southern Ocean, Nature, 373, 412–415, doi:10.1038/373412a0, 1995. 6195

Fogt, R. L., Bromwich, D. H., and Hines, K. M.: Understanding the SAM influence on the South Pacific ENSO teleconnection, Clim. Dynam., 36, 1555–1576, doi:10.1007/s00382-010-0905-0, 2011. 6204

Fritsen, C. H., Lytle, V. I., Ackley, S. F., and Sullivan, C. W.: Autumn bloom of Antarctic pack-ice algae, Science, 266, 782–784, doi:10.1126/science.266.5186.782, 1994. 6190

Garrison, D. L., Ackley, S. F., and Buck, K. R.: A physical mechanism for establishing algal populations in frazil ice, Nature, 306, 363–365, doi:10.1038/306363a0, 1983. 6194

Garrison, D. L., Close, A., and Reimnitz, E.: Algae concentrated by frazil ice: evidence from laboratory experiments and field measurements, Antarct. Sci., 1, 131–316, doi:10.1017/S0954102089000477, 1989. 6194

TCD
9, 6187–6222, 2015

Hillebrand, H., Dürselen, C.-D., Kirschtel, D., Pollingher, U., and Zohary, T.: Biovolume calculation for pelagic and benthic microalgae, J. Phycol., 35, 403–424, 1999. 6192, 6203

Hines, K. M., Bromwich, D. H., and Marshall, G. J.: Artificial surface pressure trends in the NCEP–NCAR reanalysis over the Southern Ocean and Antarctica, J. Climate, 13, 3940–3952, doi:10.1175/1520-0442(2000)013<3940:ASPTIT>2.0.CO;2, 2000. 6205

IPCC: Climate Change 2007: The Physical Science Basis, Contribution of Working Group I to the Fourth Assessment Report of the Intergovernmental Panel on Climate Change, Cambridge University Press, Cambridge, UK and New York, USA, 2007. 6204

Kang, S.-H. and Fryxell, G. A.: Phytoplankton in the Weddell Sea, Antarctica: composition, abundance and distribution in water-column assemblages of the marginal ice-edge zone during austral autumn, Mar. Biol., 116, 335–348, doi:10.1007/BF00350024, 1993. 6190

Kistler, R., Kalnay, E., Collins, W., Saha, S., White, G., Woollen, J., Chelliah, M., Ebisuzaki, W., Kanamitsu, M., Kousky, V., Dool, H. V. D., Jenne, R., and Fiorino, M.: The NCEP – NCAR 50 year reanalysis: monthly means CD-ROM and documentation, B. Am. Meteorol. Soc., 82, 247–268, 2001. 6205

Kovacs, A.: Sea Ice Part 1. Bulk salinity versus ice floe thickness, Tech. rep., CRREL, Hanover, NH, 1996. 6200

Krembs, C., Gradinger, R., and Spindler, M.: Implications of brine channel geometry and surface area for the interaction of sympagic organisms in Arctic sea ice, J. Exp. Mar. Biol. Ecol., 243, 55–80, doi:10.1016/S0022-0981(99)00111-2, 2000. 6196

L'Heureux, M. L. and Thompson, D. W. J.: Observed Relationships between the El Niño–Southern Oscillation and the Extratropical Zonal-Mean Circulation, J. Climate, 19, 276–287, doi:10.1175/JCLI3617.1, 2006. 6204

Marshall, G. J.: Trends in the Southern Annular Mode from Observations and Reanalyses, J. Climate, 16, 4134–4143, 2003. 6213

Massom, R. A. and Stammerjohn, S. E.: Antarctic sea ice change and variability – physical and ecological implications, Polar Science, 4, 149–186, doi:10.1016/j.polar.2010.05.001, 2010. 6194

Massom, R. A., Stammerjohn, S. E., Smith, R. C., Pook, M. J., Iannuzzi, R. A., Adams, N., Martinson, D. G., Vernet, M., Fraser, W. R., Quetin, L. B., Ross, R. M., Massom, Y., and Krouse, H. R.: Extreme anomalous atmospheric circulation in the West Antarctic Peninsula Region in austral spring and summer 2001/02, and its profound impact on sea ice and biota, J. Climate, 19, 3544–3571, 2006. 6189, 6191, 6194, 6195

TCD
9, 6187–6222, 2015

Massom, R. A., Reid, P., Stammerjohn, S., Raymond, B., Fraser, A., and Ushio, S.: Change and Variability in East Antarctic Sea Ice Seasonality, 1979/80–2009/10, PLoS ONE, 8, e64756, doi:10.1371/journal.pone.0064756, 2013. 6194

Meiners, K. M., Vancoppenolle, M., Thanassekos, S., Dieckmann, G. S., Thomas, D. N., Tison, J.-L., Arrigo, K. R., Garrison, D. L., McMinn, A., Lannuzel, D., van der Merwe, P., Swadling, K. M., Smith Jr., W. O., Melnikov, I., and Raymond, B.: Chlorophyll *a* in Antarctic sea ice from historical ice core data, Geophys. Res. Lett., 39, L21602, doi:10.1029/2012GL053478, 2012. 6190

Melbourne-Thomas, J., Wotherspoon, S., Raymond, B., and Constable, A.: Comprehensive evaluation of model uncertainty in qualitative network analyses, Ecol. Monogr., 82, 505–519, doi:10.1890/12-0207.1, 2012. 6216

Menden-Deuer, S. and Lessard, E. J.: Carbon to volume relationships for dinoflagellates, diatoms, and other protist plankton, Limnol. Oceanogr., 45, 569–579, doi:10.4319/lo.2000.45.3.0569, 2000. 6192, 6203

Mitchell, B. G. and Holm-Hansen, O.: Observations and modeling of the Antarctic phytoplankton crop in relation to mixing depth, Deep-Sea Res., 38, 981–1007, 1991. 6190

Mudelsee, M.: Estimating Pearson's correlation coefficient with bootstrap confidence interval from serially dependent time series, Math. Geol., 35, 651–665, doi:10.1023/B:MATG.0000002982.52104.02, 2003. 6213

Murphy, E., Cavanagh, R., Hofmann, E., Hill, S., Constable, A., Costa, D., Pinkerton, M., Johnston, N., Trathan, P., Klinck, J., Wolf-Gladrow, D., Daly, K., Maury, O., and Doney, S.: Developing integrated models of Southern Ocean food webs: Including Ecol. Complex., accounting for uncertainty and the importance of scale, Prog. Oceanogr., 102, 74–92, doi:10.1016/j.pocean.2012.03.006, 2012. 6197

Puccia, C. J. and Levins, R.: Qualitative modeling in ecology: Loop analysis, signed digraphs, and time averaging, in: Qualitative Simulation Modeling and Analysis, edited by: Fishwick, P. A. and Luker, P. A., Springer, New York, 119–143, doi:10.1007/978-1-4613-9072-5_6, 1991. 6216

Raphael, M. N.: The influence of atmospheric zonal wave three on Antarctic sea ice variability, J. Geophys. Res., 112, D12112, doi:10.1029/2006JD007852, 2007. 6204, 6213

Sarmiento, J. L. and Gruber, N.: Ocean Biogeochemical Dynamics, Princeton University Press, Princeton, 2006. 6199

TCD
9, 6187–6222, 2015

Sarthou, G., Timmermans, K. R., Blain, S., and Tréguer, P.: Growth physiology and fate of diatoms in the ocean: a review, J. Sea Res., 53, 25–42, doi:10.1016/j.seares.2004.01.007, 2005. 6198

Shrestha, D. L., Robertson, D. E., Wang, Q. J., Pagano, T. C., and Hapuarachchi, H. A. P.: Evaluation of numerical weather prediction model precipitation forecasts for short-term streamflow forecasting purpose, Hydrol. Earth Syst. Sci., 17, 1913–1931, doi:10.5194/hess-17-1913-2013, 2013. 6202

Smith Jr., W. O. and Nelson, D. M.: Phytoplankton growth and new production in the Weddell Sea marginal ice zone in the austral spring and autumn, Limnol. Oceanogr., 35, 809–821, doi:10.4319/lo.1990.35.4.0809, 1990. 6190

Smith Jr., W. O., Marra, J., Hiscock, M. R., and Barber, R. T.: The seasonal cycle of phytoplankton biomass and primary productivity in the Ross Sea, Antarctica, Deep-Sea Res. Pt. II, 47, 3119–3140, doi:10.1016/S0967-0645(00)00061-8, 2000. 6190

Vance, T. R., van Ommen, T. D., Curran, M. A. J., Plummer, C. T., and Moy, A. D.: A millennial proxy record of ENSO and eastern Australian rainfall from the Law Dome Ice Core, East Antarctica, J. Climate, 26, 710–725, doi:10.1175/JCLI-D-12-00003.1, 2013. 6204

Vancoppenolle, M., Goosse, H., de Montety, A., Fichefet, T., Tremblay, B., and Tison, J.-L.: Modeling brine and nutrient dynamics in Antarctic sea ice: The case of dissolved silica, J. Geophys. Res., 115, C02005, doi:10.1029/2009JC005369, 2010. 6197

van der Merwe, P., Lannuzel, D., Bowie, A. R., and Meiners, K. M.: High temporal resolution observations of spring fast ice melt and seawater iron enrichment in East Antarctica, J. Geophys. Res., 116, G03017, doi:10.1029/2010JG001628, 2011. 6196

van Ommen, T. D. and Morgan, V.: Snowfall increase in coastal East Antarctica linked with southwest Western Australian drought, Nat. Geosci., 3, 267–272, doi:10.1038/ngeo761, 2010. 6205, 6213

Winton, V. H. L., Dunbar, G. B., Bertler, N. A. N., Millet, M.-A., Delmonte, B., Atkins, C. B., Chewings, J. M., and Andersson, P.: The contribution of aeolian sand and dust to iron fertilization of phytoplankton blooms in southwestern Ross Sea, Antarctica, Global Biogeochem. Cy., 28, 423–436, doi:10.1002/2013GB004574, 2014. 6195

TCD
9, 6187–6222, 2015

Table D1. Biological characteristics of opportunistic samples.

		Samples of sea ice-associated bloom							
	Sample	V4-001		V4-002		V4-003		V4-004	
	Longitude; Latitude	67°51′ S; 66°42′ E		67°05′ S; 66°02′ E		67°20′ S; 66°55′ E		67°08′ S; 67°27′ E	
	Chlorophyll *a* [mg m^{-3}]	Mean	SE	Mean	SE	Mean	SE	Mean	SE
		0.33	0.12	2.77	0.37	2.24	0.52	1.34	0.25
	Abundance [Cells L^{-1}]	Mean	SE	Mean	SE	Mean	SE	Mean	SE
Totals	Total Cells	1 284 776	79 812	786 101	34 614	1 355 564	57 488	2 559 239	121 069
	Total autos	927 197	68 610	486 588	24 477	914 533	48 436	1 844 402	70 108
	Total Het	357 580	29 646	299 513	15 972	441 031	20 724	714 837	67 791
Autotrophs	*Chaetoceros* spp	969	667	12 116	2973	21 325	4196	17 447	2289
	Fragilariopsis < 20	467 347	47 419	116 800	13 202	315 991	22 474	552 985	38 249
	Fragilariopsis > 20	58 158	8641	181 743	18 295	347 009	29 723	623 744	45 395
	Other centrics	3393	1454	19 386	3852	17 932	2142	17 932	2657
	Other pennates	19 871	2766	35 379	4986	43 618	3947	79 967	6885
	Phaeocystis	306 783	47 111	52 827	6386	73 667	6344	313 879	36 621
	Auto flag	64 376	7933	29 564	5646	42 164	5937	40 711	4254
	Dactyliosolen tenuijunctus	6785	1588	38 772	4392	52 827	6386	197 737	13 679
Heterotrophs	*Gyrodinium*	18 901	2766	2423	1973	5331	1488	5331	1645
	Other Het Dinos	7270	1553	53 796	5142	58 643	3882	44 103	3182
	Unk Flg (mainly HNAN)	283 428	30 299	205 007	13 513	218 577	14 195	531 721	63 609
	Choanos	2908	1737	10 178	2165	14 055	1923	9208	2276
	Cryptos	44 103	2940	20 840	2464	76 090	7451	52 827	5045
	Ciliates	0	0	485	485	969	667	485	485
	Other het Flg	969	667	6785	1874	67 366	7718	71 162	4652
	Biomass [mg C L^{-1}]	Mean	SE	Mean	SE	Mean	SE	Mean	SE
Totals	Total Cells	53	4	90	8	132	8	557	27
	Total autos	43	3	63	6	93	7	532	26
	Total Het	10	2	27	4	40	5	25	3
Autotrophs	*Chaetoceros* spp	0	0	1	0	1	0	4	1
	Fragilariopsis < 20µm	14	1	4	1	14	1	70	6
	Fragilariopsis > 20µm	5	1	20	2	37	3	186	13
	Other centrics	5	3	6	3	4	2	5	1
	Other pennates	3	1	8	2	8	2	27	3
	Phaeocystis	2	0	0	0	1	0	2	0
	Auto flag	12	2	7	3	6	2	2	0
	Dactyliosolen tenuijunctus	3	1	16	2	22	3	235	16
Heterotrophs	*Gyrodinium*	3	1	3	2	7	2	7	2
	Other Het Dinos	4	1	22	3	27	4	11	2
	Unk Flg (mainly HNAN)	2	0	1	0	1	0	3	0
	Choanos	0	0	0	0	0	0	0	0
	Cryptos	1	0	0	0	1	0	1	0
	Ciliates	0	0	0	0	1	1	0	0
	Other het Flg	0	0	1	0	3	0	3	0

TCD
9, 6187–6222, 2015

Table D1. Continued.

	Sample Latitude; Longitude	V4-005 66°57′ S; 67°58′ E		V4-006 66°43′ S; 68°29′ E		V4-007 66°34′ S; 68°46′ E		Mean inside Bloom	Mean outside Bloom
	Chlorophyll *a* [mg m^{-3}]	Mean 1.09	SE 0.09	Mean 0.79	SE 0.07	Mean 0.45	SE 0.02	2.11	0.66
	Abundance [Cells L^{-1}]	Mean	SE	Mean	SE	Mean	SE		
Totals	Total Cells	1 211 268	121 565	1 271 930	40 302	1 754 621	115 764	1 566 968	1 380 649
	Total autos	662 987	56 356	1 004 249	38 811	1 205 935	70 878	1 081 841	950 092
	Total Het	548 281	79 677	267 681	22 826	548 686	70 623	485 127	430 557
Autotrophs	*Chaetoceros* spp	1939	1939	3393	2562	969	667	16 963	1817
	Fragilariopsis < 20	356 125	47 448	529 137	33 735	899 072	52 931	328 592	562 920
	Fragilariopsis > 20	76 090	13 310	30 533	6828	1454	1454	384 165	41 559
	Other centrics	5331	1789	11 632	4481	12 116	2423	18 417	8118
	Other pennates	17 932	3535	15 024	2766	9693	1861	52 988	15 630
	Phaeocystis	101 776	20 411	216 638	22 428	245 232	40 817	146 791	217 607
	Auto flag	24 717	5238	180 445	35 132	18 012	5471	37 480	71 888
	Dactyliosolen tenuijunctus	11 147	2142	15 993	2023	18 901	3752	96 445	13 207
Heterotrophs	*Gyrodinium*	9208	2165	9693	2436	13 570	2156	4362	12 843
	Other Het Dinos	8239	2361	17 447	3627	12 116	4328	52 181	11 268
	Unk Flg (mainly HNAN)	501 270	79 278	192 076	24 008	489 558	71 087	318 435	366 583
	Choanos	485	485	4846	1793	2908	1238	11 147	2787
	Cryptos	28 110	5066	43 134	3259	29 564	2581	49 919	36 228
	Ciliates	485	485	485	485	485	485	646	363
	Other het Flg	485	485	0	0	485	485	48 438	485
	Biomass [mg C L^{-1}]	Mean	SE	Mean	SE	Mean	SE		
Totals	Total Cells	71	10	88	9	99	13	260	78
	Total autos	57	9	74	9	86	12	229	65
	Total Het	15	3	14	3	12	2	31	13
Autotrophs	*Chaetoceros* spp	1	1	0	0	0	0	2	0
	Fragilariopsis < 20µm	11	1	18	1	31	2	30	18
	Fragilariopsis > 20µm	5	1	3	1	0	0	81	3
	Other centrics	12	6	28	9	38	10	5	21
	Other pennates	3	2	2	1	3	1	14	3
	Phaeocystis	1	0	1	0	1	0	1	1
	Auto flag	3	1	13	3	5	2	5	8
	Dactyliosolen tenuijunctus	5	1	7	1	8	2	91	6
Heterotrophs	*Gyrodinium*	5	2	5	1	3	1	5	4
	Other Het Dinos	3	1	5	2	5	2	20	4
	Unk Flg (mainly HNAN)	3	0	2	1	3	0	2	2
	Choanos	0	0	0	0	0	0	0	0
	Cryptos	4	1	2	0	1	0	1	2
	Ciliates	0	0	0	0	0	0	0	0
	Other het Flg	0	0	0	0	0	0	2	0

TCD
9, 6187–6222, 2015

Table G1. Correlation of summer SOI November to February (NDJF) with SAM [Marshall, 2003] and the Australian sector ZW3 (AZ3) for December to March (DJFM) (van Ommen and Morgan, 2010). Monthly SOI is from the Bureau of Meteorology (BOM) Australia data. The SAM index monthly data is after Marshall (2003). The AZ3 index is an Australian sector ZW3 index (Raphael, 2007) and is computed from the difference in annual average 500 hPa GPH averaged over two boxes (155 to 160° E and 110 to 115° E, both extending from 45 to 65° S) (van Ommen and Morgan, 2010). Correlations are calculated using detrended time series and errors are bootstrap confidence intervals (Mudelsee, 2003). Two-tailed significance is stated from effective degrees of freedom (N^{eff}) calculated from lag 1 autocorrelation of both series. It is worth noting that if March is left off the summer SAM composite the correlation, though still significant, declines (from $p = 0.004$ to $p = 0.01$).

Index (detrended) (DJFM)	Range	r	95 % CI	Significance
SAM	1958–2012	0.383	[0.151; 0.571]	0.004, $N^{\text{eff}} = 56$
AZ3	1958–2005	0.509	[0.250; 0.708]	0.0002, $N^{\text{eff}} = 48$

TCD
9, 6187–6222, 2015

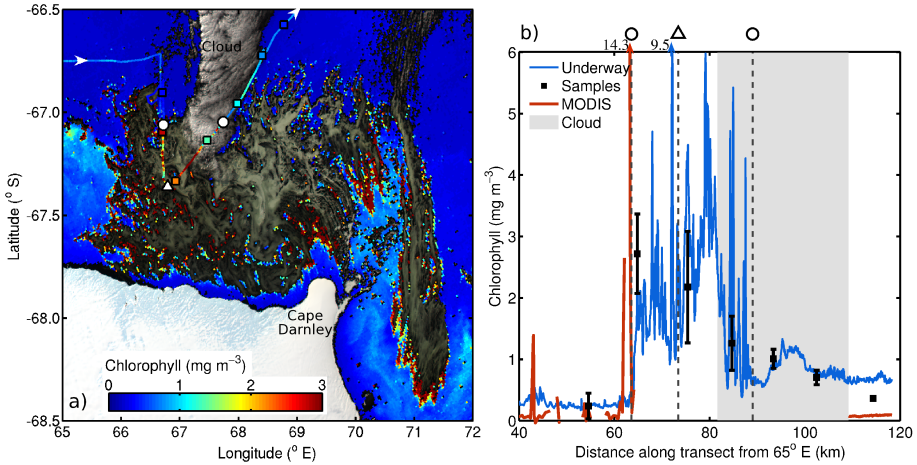

Figure 1. (a) Combined satellite image of the bloom using MODIS true-color (channels 1, 4 and 3) and ocean-color (channels 9, 10 and 12) bands (primary color scale: mg m^{-3}) dated 2 March 2012 10:30 UTC. True-color imagery of discolored sea ice (and clouds) replaces the area flagged as ice (and cloud) by the standard Chl *a* algorithm. Also shown is the ship track with underway Chl *a* data calculated from fluorometry and corresponding mean of the seawater samples (colored squares). White arrowheads indicate the cruise direction. The zone where the ship is within sea ice is bounded by the circles and the triangle indicates where the ship changed course (meanings are the same for **b**). **(b)** Transect of underway Chl *a* estimates calculated from fluorometry (blue line), and mean and standard deviation of the samples (black lines) used to calibrate these, compared with the MODIS values (discontinuous red line) which are affected by masking due to the presence of both cloud (grey zone) and sea ice.

TCD
9, 6187–6222, 2015

Figure 2. Photograph from the ship of the early autumn bloom, taken on 5 March 2012 at approximately 67.25° S and 67.16° E; field of view is approximately 3 m × 5 m (photo courtesy: Nobuo Kokubun, AAD).

TCD
9, 6187–6222, 2015

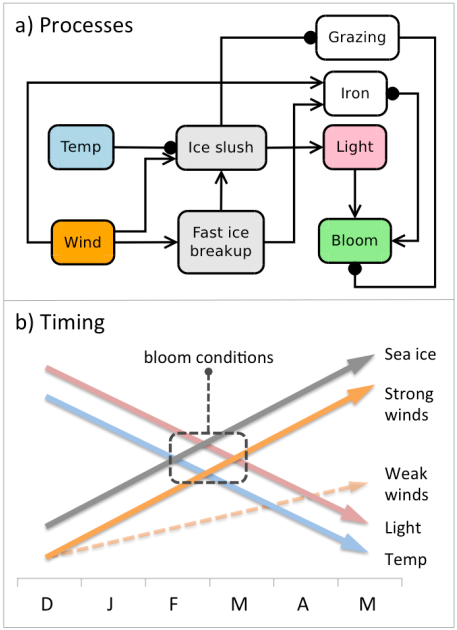

Figure 3. (a) Conceptual model illustrating the interactions between proximal drivers leading to conditions favouring early autumn ice-associated blooms in the Southern Ocean. Connections terminating in an arrow indicate a positive effect from one model component to another, while those ending in a filled circle indicate a negative effect (following the syntax for signed directed graphs in qualitative network analysis; Puccia and Levins, 1991; Melbourne-Thomas et al., 2012). Two-ways feedback is also possible. Decreases in atmospheric temperature (blue) and increases in wind (orange) promote the formation of ice slush, which, together with iron released from wind-induced upwelling and fast ice breakup, promotes the formation of early autumn blooms (green). **(b)** The corresponding timing of changes in levels of light, sea ice, atmospheric and sea-surface temperature and wind strength for the Cape Darnley region between December and May. Optimal conditions for bloom formation overlap in late February/early March.

TCD
9, 6187–6222, 2015

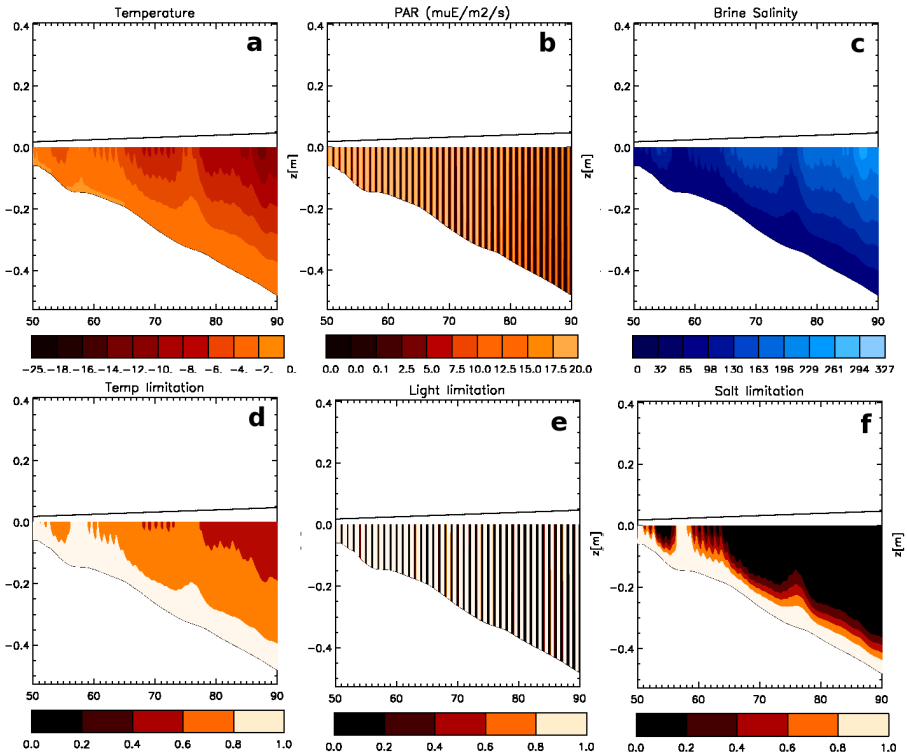

Figure A1. Physical ice features simulated by the model in all four runs, **(a)** temperature, **(b)** light in quantum units, **(c)** brine salinity, and the associated limitation factors **(d–f)**.

TCD
9, 6187–6222, 2015

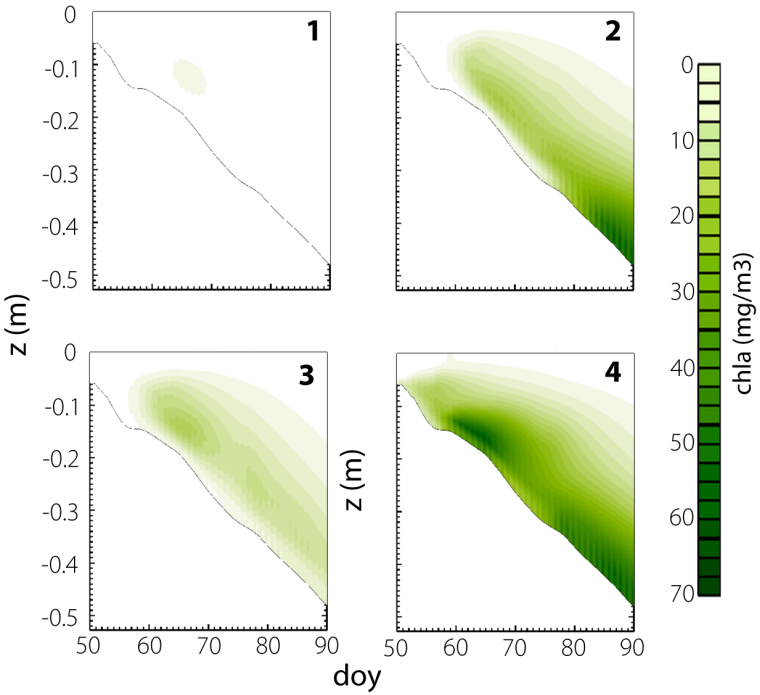

Figure A2. Simulated Chl *a* development from Experiments 1 to 4.

TCD
9, 6187–6222, 2015

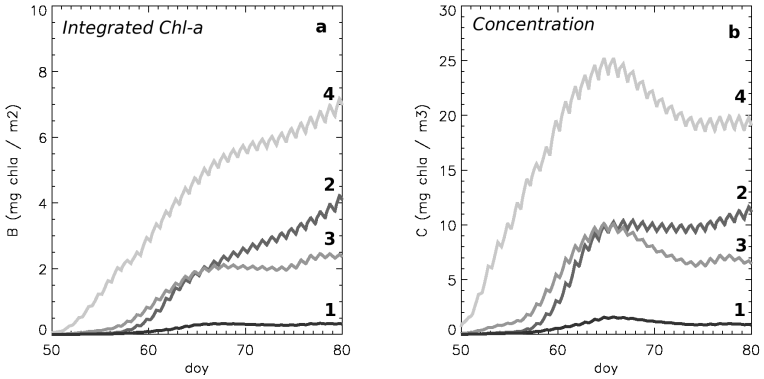

Figure A3. Simulated Chl *a* development **(a)**, vertically integrated; **(b)** vertical-mean concentration, for Experiments 1 to 4.

TCD
9, 6187–6222, 2015

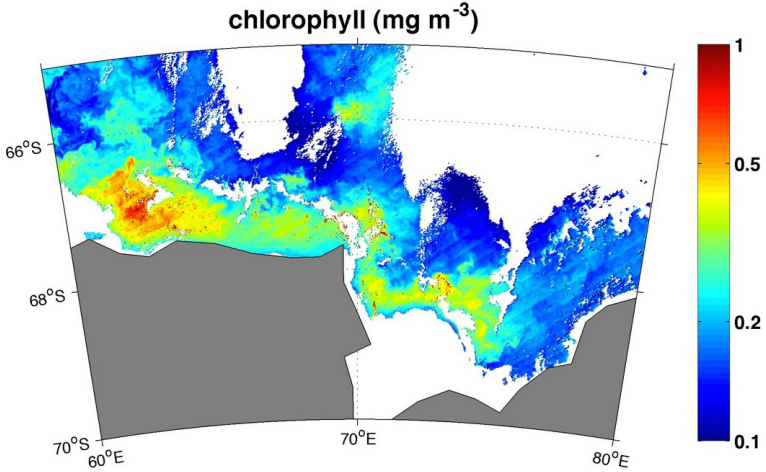

Figure E1. MODIS ocean-colour before ice associated bloom (11 February 2012) to show existing primary production.

TCD
9, 6187–6222, 2015

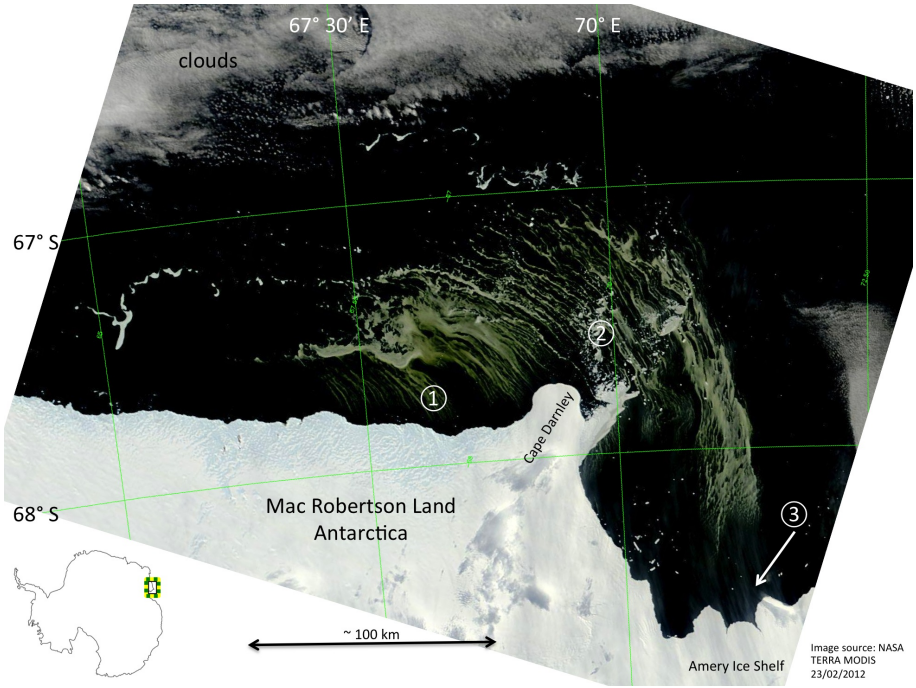

Figure F1. MODIS true-colour image, illustrating potential ice seeding mechanisms, including (1) wind-driven formation of strips and patches, (2) disintegrating fast ice, and (3) wind-blown snow off the face of the Amery Ice Shelf.

TCD
9, 6187–6222, 2015

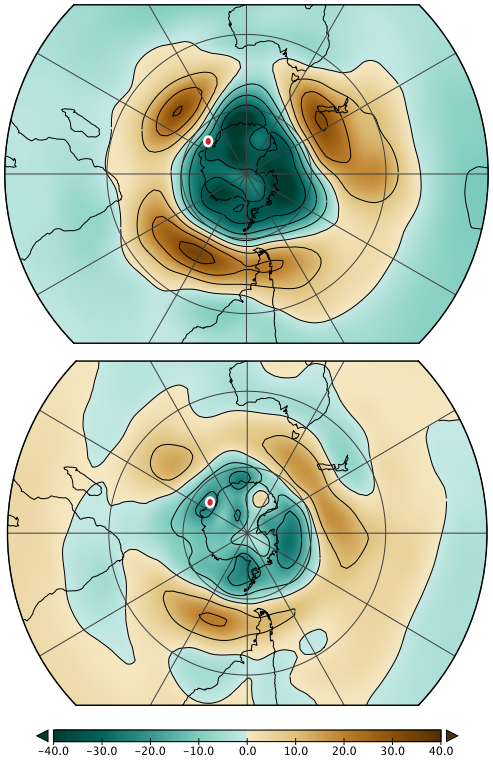

Figure G1. Composite images of 500 hPa geopotential height (GPH500) anomalies from December to March. Upper panel: composite of years that are coincident in both the upper quartile of Southern Oscillation Index (November to February) and SAM (December to March) averaged summer values (1979–2012) are composited. Lower panel: composite of bloom years identified by satellite images from 2000–2012 (December to March). Cape Darnley region is identified with a red dot. Contours are 10 m.

TCD
9, 6187–6222, 2015